Journal Pre-proof

Variation of contact resonance frequency during domain switching in PFM measurements for ferroelectric materials

Yue Liu, Yao Sun, Wanheng Lu, Hongli Wang, Zhongting Wang, Bingxue Yu, Tao Li, Kaiyang Zeng

PII: S2352-8478(19)30151-0

DOI: https://doi.org/10.1016/j.jmat.2019.12.011

Reference: JMAT 259

To appear in: *Journal of Materiomics*

Received Date: 8 September 2019

Revised Date: 16 November 2019

Accepted Date: 24 December 2019

Please cite this article as: Liu Y, Sun Y, Lu W, Wang H, Wang Z, Yu B, Li T, Zeng K, Variation of contact resonance frequency during domain switching in PFM measurements for ferroelectric materials, *Journal of Materiomics* (2020), doi: https://doi.org/10.1016/j.jmat.2019.12.011.

Graphical Abstract

Variation of Contact Resonance Frequency during Domain Switching in DART-PFM Measurements for Ferroelectric Materials

Yue Liu, Yao Sun, Wanheng Lu, Hongli Wang, Zhongting Wang, Bingxue Yu, Tao Li,[*,#] *Kaiyang Zeng*[*]

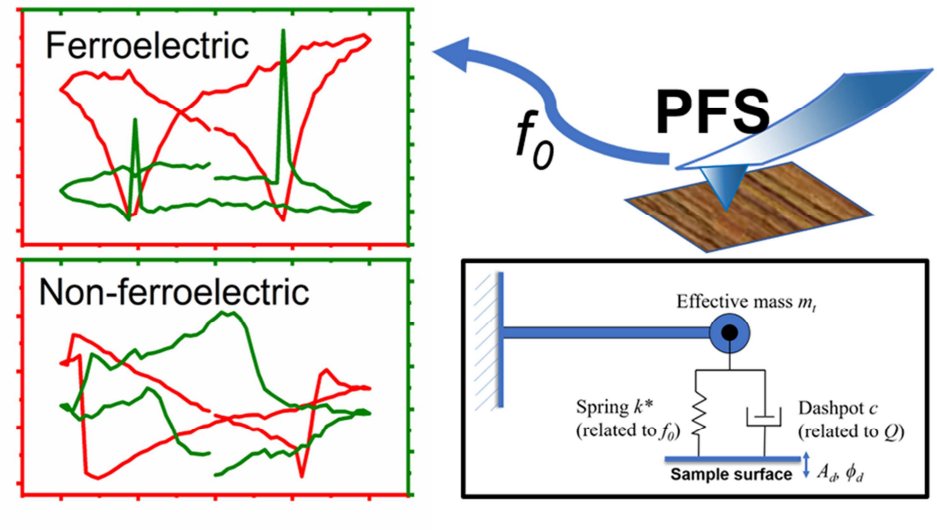

Variation of Contact Resonance Frequency during Domain Switching in PFM Measurements for Ferroelectric Materials

Yue Liu, Yao Sun, Wanheng Lu, Hongli Wang, Zhongting Wang, Bingxue Yu, Tao Li,[*,#] *Kaiyang Zeng*[*]

* E-mail: mpezk@nus.edu.sg； taoli66@xjtu.edu.cn.

Department of Mechanical Engineering, National University of Singapore, 9 Engineering Drive 1, Singapore 117576

Current address: Center for Spintronics and Quantum System, State Key Laboratory for Mechanical Behavior of Materials, School of Materials Science and Engineering, Xi'an Jiaotong University, Shanxi 710049, Xi'an, China.

KEYWORDS: ferroelectricity, Piezoresponse Force Spectroscopy, contact resonance frequency, dual AC resonance tracking, domain switching, damping harmonic oscillator model

ABSTRACT: Piezoresponse Force Spectroscopy (PFS) is a powerful technique widely used for measuring the nanoscale electromechanical coupling of the ferro-/piezo-electric materials. However, it is found that certain non-ferroelectric materials can also generate the "hysteresis-loop-like" responses from the PFS measurements due to many other factors such as electrostatic effects. This work therefore studies the signal of the contact resonance frequency during the PFS measurements. By comparing the

results from ferroelectric and non-ferroelectric materials, it is found there are distinct differences between these two types of materials in the variation of the contact resonance frequency during the PFS measurements. A momentary and sharp increase of the contact resonance frequency occurs when the domain is switched by applying the DC bias, which can be regarded as a unique characteristic for the ferroelectric materials. After analyzing the reliability and mechanism of the method, it is proposed that the contact resonance frequency variation at the coercive bias is capable to differentiate the electromechanical responses of the ferroelectric and non-ferroelectric materials during the PFS measurements.

INTRODUCTION

Development and applications of the ferroelectric materials have been one of the most active topics for decades. Due to the unique characteristics of spontaneous polarization, ferroelectric materials have been used in a wide range of applications, such as sensors, actuators and memory devices [1,2]. Developing new ferroelectric materials has great significances for research and applications in the area of functional materials [3,4]. To study the ferroelectric behavior at nanoscale, Piezoresponse Force Microscopy (PFM) and its spectroscopy form, Piezoresponse Force Spectroscopy (PFS), are widely used in the last decades [5–9]. As the premier characterization tools for domain structures and orientation as well as nano-scale properties of the ferroelectric materials, PFM and PFS techniques can probe time- or voltage-dependent phenomena with high spatial resolution [8,10–12]. In the PFS measurements, the surface of the sample contacts with a sharp conductive tip at the end of a PFM cantilever. After applying excitation of DC pulse from the tip to the sample surface, the local polarization switching may occur and can be detected by the same tip. Because of the nonlinear

piezoelectric responses, the *PR* curve forms a closed hysteresis loop under the cyclic DC voltage sweeping, which is regarded as a general electromechanical response from the ferroelectric materials [13]. The shape of an electromechanical hysteresis loop depends on the properties of the material and the experimental conditions [14]. Therefore, yielding a hysteresis loop in the PFS measurement in the off-field is generally a well-recognized evidence for ferroelectricity on the range from nanoscale to macroscale [5,8,14].

However, the measurements of the local ferroelectric responses can be affected by a number of factors [15]. Besides the polarization-electric field (P-E) relationship, the electrostatic force between the tip and sample surface [16], surface charging [9,17,18], Vegard effect [19] and ionic mechanisms [20–22] can also induce the "hysteresis-loop-like" responses in which are similar to the P-E loops obtained in ferroelectric materials during the PFS measurements. Therefore, such "hysteresis-loop-like" behaviors can also be observed in a broad variety of non-ferroelectric materials during the PFS measurements, for example, glass [23], $LiCoO_2$ [20], TiO_2 [24] and even banana peel [25]. It is therefore believed that the hysteresis loop obtained by PFS is insufficient as the only proof of the ferroelectricity [26]. Due to these facts, numbers of other methods to probe the local ferroelectric phenomena have been developed in the recent years. These methods usually introduce different techniques other than PFS (or its mapping technique as Switching Spectroscopy Piezoresponse Force Microscopy, SS-PFM) to investigate the ferroelectric characteristics. For example, optical second harmonic generation (SHG) can differentiate ferroelectric and magnetic phase transitions by using the light beams with different incident wavelengths [27,28]. Ultraviolet Raman Spectroscopy [29] and unit-cell scale mapping [30] also provide the evidence for nanoscale ferroelectricity. On the other hand, contact Kelvin Probe Force Microscopy (cKPFM) [31] and frequency dependent PFM [32] are developed as the effective new measurements to differentiate the true ferroelectricity contributions with the combination of hysteresis loops in PFS measurements. Furthermore, various techniques with higher harmonic frequencies are also developed to distinguish the responses from the ferroelectric and non-

ferroelectric materials [19]. Most of those experimental techniques are relatively complicated and require new set-ups, methods or analysis, because the PFM/PFS technique alone is insufficient to determine if the responses are real ferroelectric for an unknown material. On the other hand, almost all of the PFS (or SS-PFM) studies only analyze the amplitude and the phase angle changes induced by the external electric field, while other parameters during the PFS measurements are largely ignored. Especially, the contact resonance frequency (f_0) and quality factor (Q) obtained during the PFS measurements are not carefully considered in the analysis published so far.

In this study, we first report that the contact resonance frequency signal, f_0, shows a unique pattern in ferroelectric materials whereas the non-ferroelectric materials do not show such pattern. It is therefore believed that such unique pattern may be related to the mechanical properties of ferroelectric materials. Hence, a simple yet effective method is proposed based on the changes of f_0 during the PFS measurements, which can be used to simply differentiate ferroelectric material and non-ferroelectric material with hysteresis-like loops. In addition, the artifacts analysis validates that the variation of contact resonance frequency in the PFS measurements is a stable and significant feature for ferroelectric materials. This method also provides a new perspective to understand the PFS signals and the properties of ferroelectric materials.

MATERIALS AND EXPERIMENTS

In this work, three groups of eight materials were tested, including four ferroelectric materials, two non-ferroelectric materials with PFS measured hysteresis loops, and two non-ferroelectric materials without any hysteresis loops can be measured from the PFS experiments. The ferroelectric materials included $Pb(Zn_{1/3}Nb_{2/3})O_3$–9%$PbTiO_3$ (PZN–PT) single crystals, hybrid polymeric–metallic (PVDF–Ag) composite, $BiFeO_3$ (BFO) and 2%Cu-doped ZnO film. The preparations of the PZN-PT, PVDF-Ag and ZnO samples were described in the previous studies [33–35]. The preparation of the BFO sample

was discussed in Ref. [36]. The non-ferroelectric samples were glass and banana peel. The glass sample was a glass cover slip (type:72210-10, Electron Microscopy Science, USA). The banana peel sample was sliced from a fresh banana's outside surface and dried for 12 hours. The pure silicon (Si) sample was a commercial material (Silicon Valley Microelectronics, USA). The Poly(methyl methacrylate) (PMMA) sample was also commercially available material (Goodfellow Ltd, UK).

The PFS measurements were conducted using a commercial SPM system (MFP-3D, Oxford Instruments, CA, USA), in Dual-AC Resonance Tracking (DART) mode. Two types of tips were used for measurements on different materials. The SPM tips used in the PFS measurements and their information are listed in Table 1.

Table 1. SPM Tips used in this study and their information (by manufacturer).

SPM Tip	Resonance Frequency (f_c) /kHz	Spring Constant (k_c) /(N/m)	Sample
PPP-NCSTPt (Nanoworld, Switzerland)	~160	~7.4	PZN-PT
			BFO
			Glass
			Banana peel
			PMMA
240AC-PP (Nanoworld, Switzerland)	~70	~2	PVDF-Ag
			ZnO
			Si

RESULTS

Variation of f_0 during the PFS measurements

In order to investigate the relationships between the piezoresponse *(PR)* and f_0 in ferroelectric and non-ferroelectric materials, we first re-plot the data as *PR* versus f_0 plots. In this plot, the x-axis is

PR responses based on experimentally obtained PFS amplitude and phase angle) and the y-axis is f_0. The local off-field hysteresis loops and amplitude loops of the ferroelectric materials can be seen in Figs. 1(a), (c), (e) and (g). The signal of amplitude is mainly affected by the deformation of the sample surface due to the bias field. The relationships between off-field *PR* and f_0 of these materials are shown in Figs. 1(b), (d), (f) and (h). It is illustrated that, in the ferroelectric materials including the Cu-doped ZnO, when the applied DC voltage reaches the coercive bias, f_0 jumps to a notably high value suddenly; and after the coercive bias, f_0 reverts to the values as before. This pattern occurs twice in a bias cycle at the two coercive biases. The data, including A_1, f_1, DHO calculated ϕ_d, A_1/A_2 ratio and the DART frequency width (defined as f_2-f_1, and this DART frequency width is termed as DFW in this paper), is shown in Fig. S1 (Supporting Information, SI). In short, all of the ferroelectric materials tested here show two sharp peaks in the *PR*-f_0 curves at the position where *PR* nearly equals to zero.

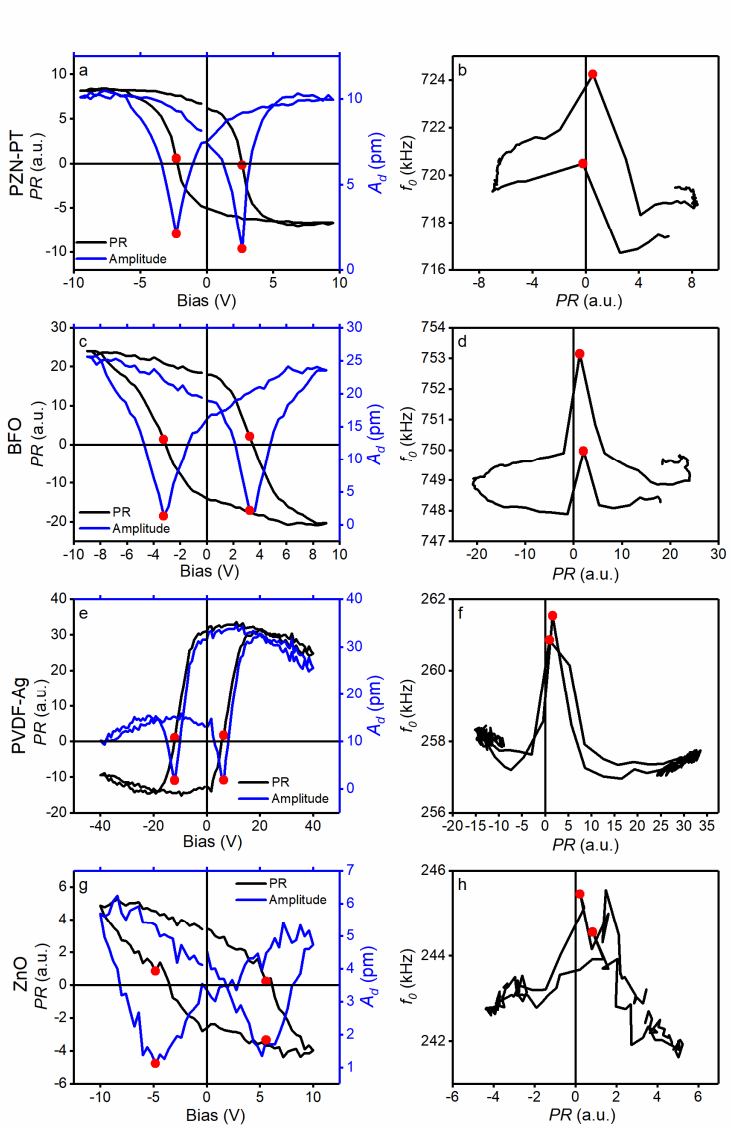

Fig. 1. PFS amplitude loop (measured at off-field) and calculated hysteresis loop for ferroelectric materials: (a) PZN-PT, (c) BFO, (e) PVDF-Ag and (g) Cu-doped ZnO. Contact resonance frequency as function of calculated piezoresponse (*PR*-f_0) for (b) PZN-PT, (d) BFO, (f) PVDF-Ag and (h) Cu-doped ZnO at off-field. The red dots in (b), (d), (f) and (h) highlight the peak positions in the *PR*-f_0 loop. The points marked by red dots in (a), (c), (e) and (g) show the corresponding *PR* and amplitude where the contact resonance frequencies reach to the peak values, respectively.

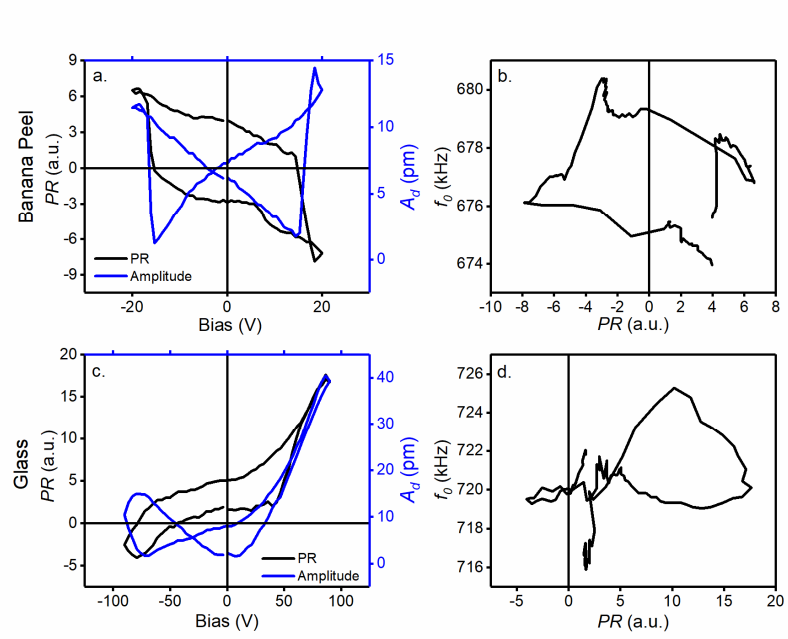

Fig. 2. PFS amplitude loop (measured at off-field) and calculated hysteresis-like loops for some non-ferroelectric materials with PFS measured amplitude and phase loops: (a) banana peel and (c) glass. Contact Resonance Frequencies as function of calculated piezoresponse (*PR*-f_0) loops for (b) glass and (d) banana peel measured at off-field. Note there are no contact resonance frequency peaks and any regular patterns for the curves in those materials.

It is known that some non-ferroelectric materials also demonstrate ferroelectric-like hysteresis loops and amplitude loops during the PFS measurements, such as glass and banana peel, which can be seen in Figs. 2(a) and (c). The corresponding *PR*-f_0 curves are shown in Figs. 2(b) and (d). Obviously, the *PR*-f_0 curves are significantly different between the ferroelectric materials and the non-ferroelectric materials. Most importantly, no f_0 peaks are observed in the PFS measurements of the glass and banana peel samples at the positions around their "coercive bias". Each of the non-ferroelectric material has random f_0 signals. Similarly, more data of A_1, f_1, DHO calculated ϕ_d, A_1/A_2 ratio and different DFWs is shown in Fig. S2 (SI). In other words, despite the observed ferroelectric-like amplitude and phase loops, non-ferroelectric materials show obvious different f_0 signals during the PFS measurements.

Furthermore, we also conducted the PFS measurements on two other non-ferroelectric materials (bulk PMMA and Si), which can be seen in Fig. S3 (SI); however, the PFS measurements cannot get any hysteresis-like loops in these two materials. As expected, the *PR*-f_0 curves are highly random and no peaks can be observed. Their behaviors during the PFS measurements are also clearly different from that of the ferroelectric materials.

To further understand the effect of DART for the PFS measurements, Fig. 3 shows the PFS measurements on PZN-PT, BFO and glass with different DFWs. The corresponding amplitude and *PR* can be seen in Fig. S4 (SI). All of those materials can obtain the hysteresis loops of the piezoresponse and "butterfly-shape" amplitude loop during the PFS measurements (Fig. 3). The tuned peaks of three materials can be seen in Fig. S5 (SI). It is shown that, for the three materials, the full width at half maximum (FWHM) of the tuned peaks are around 12 kHz. As the typical ferroelectric materials, PZN-PT and BFO show the similar behavior, i.e., the f_0 peaks occur at different DFWs. At the small DFW, f_0 peaks from PZN-PT and BFO are not as distinctive as that at the larger DFW, but the peaks still exist. However, for glass, there are no peaks at any DFW.

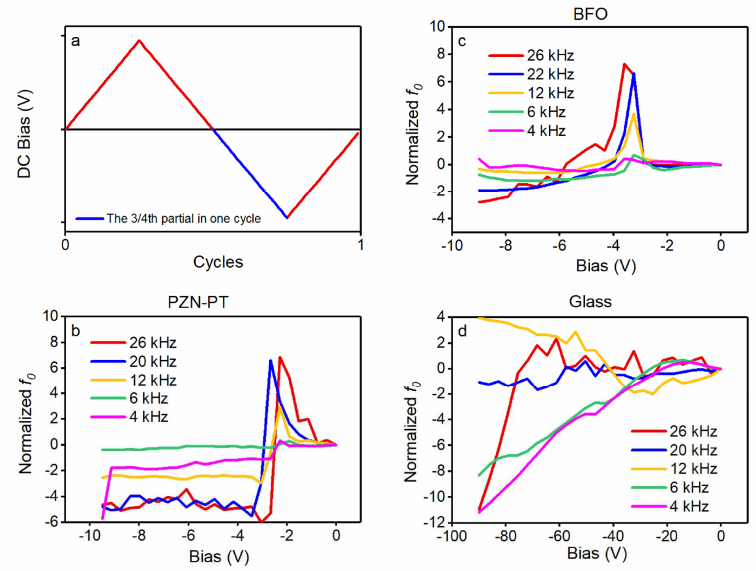

Fig. 3. Contact resonance frequency (f_0) at different DFWs of the DART measurements for (b) PZN−PT, (c) BFO, and (d) glass. (a) Bias-cycle plot shows the applied DC bias in the PFS measurements on three samples. Each sample experiences an entire cycle, but only the data in the ¾ partial (blue line in (a)) is shown here in order to observe peaks clearly. The same tip is used among different DFW measurements on each material.

In the pulsed DC mode, piezoresponses are measured respectively when the switching DC bias is on (on-field) and off (off-field) [37]. At the on-field, the applied DC voltage induces the piezoelectric motion of the domain and domain walls, and then ferroelectric materials keep this stable status at the following off-field. The off-field signal is usually considered as the clear response of the tip-sample interaction without the influences from strong DC field-induced tip-sample electrostatic interaction. Generally-speaking, the PFS measurements can obtain the variation of amplitude and the phase angle as functions of the DC bias [38]. In order to investigate the electrostatic effects on the f_0 signals, the comparison between the off-field signals and the on-field signals is shown in Fig. 4. By plotting the bias-f_0 relationship, the bias induced f_0 peaks can be clearly seen. For ferroelectric materials, in Figs. 4(a) to (d), the applied electric field significantly affects the f_0, changing the position and the height of

the peaks. However, for non-ferroelectric materials, in Figs. 4(e) and (f), the off-field and on-field curves are highly similar, with no peak can be found. Hence, it is obvious that the hysteresis loops of glass and banana peel are not associated with the "domain motion". The main factors which contribute to the hysteresis-like loops in those materials may be the electrostatic effects, presumably by the similarity between the off-field and on-field f_0 signals during the PFS measurements.

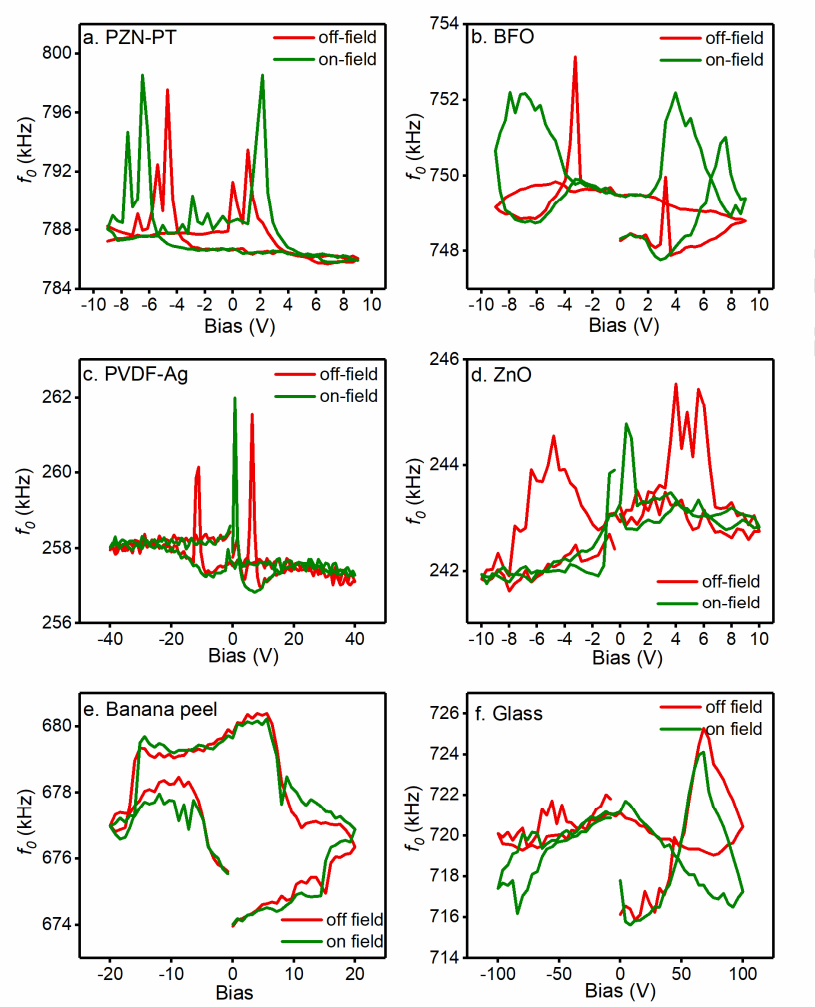

Fig. 4. Comparison between the off-field (red line) and the on-field (green line) bias-f_0 curves. Four ferroelectric materials, (a) PZN-PT, (b) BFO, (c) PVDF-Ag and (d) ZnO, are involved; two non-ferroelectric materials, (e) banana peel and (f) glass, are involved. Note that, the bias-f_0 curves from non-ferroelectric materials demonstrate highly similarity between off-field and on-field, whereas it is different from ferroelectric materials.

Furthermore, ten (10) cycles of PFS measurements have been conducted on both ferroelectric and non-ferroelectric materials to test the endurance of the f_0 signals. The wavelets analysis (by using MATLAB) is used to remove the details in f_0 and only focus on the main trend of f_0 signals as functions of PFS cycles. The sixth order approximation signals after Wavelet Daubechies (db4) transform are shown in Fig. 5 for ferroelectric and non-ferroelectric materials. Daubechies Wavelets, known as "compact support orthogonal wavelets", in which can decompose data into approximations and details without gap or overlap, is used to detect or filter the nonlinear or instantaneous response signal processing [39]. To obtain the clear trend of each sample and compare them, the signals have been normalized by the initial value of the time sequence during the PFS measurements. In all the cases, the f_0 signals are unstable in the first cycle, but they tend to be stable after 2 or 3 cycles. For glass and banana peel in the PFS measurements, the endurance of f_0 are similar to PMMA and Si which do not show hysteresis loops of piezoresponse in the ten cycles.

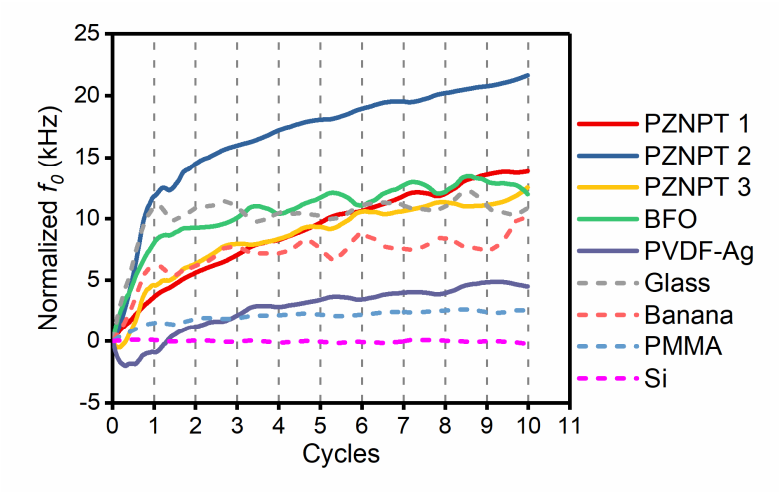

Fig. 5. Analysis of the trend of the contact resonance frequency (f_0) curves for both ferroelectric and non-ferroelectric materials by using wavelet transformation: 10 cycles of PFS measured f_0 signals (measured at off-field) after 6th approximation of the wavelets transform. The solid lines represent three individual tests on PZN-PT (ferroelectric material) samples. The dash lines represent the test data on non-ferroelectric materials of glass, banana, PMMA and Si, respectively. Note that the trend of the contact resonance curves of PZN-PT, BFO and PVDF-Ag show increasing continuously with the testing cycles, whereas, for non-ferroelectric materials, after the initial cycle, the trend of f_0 curves become independent of the testing cycles. The wavelet analysis is performed by using MATLAB (R2016b).

Because the PFS measurement is a local measurement, we conduct the repetitive measurements at five randomly selected locations, and the *PR*-f_0 curves from PZN-PT, BFO, PVDF-Ag, ZnO, glass, and banana peel are shown in Fig. S6 (SI). In addition, we also conduct the PFS mapping on two typical ferroelectric materials, PZN-PT and BFO, to prove the robustness of the variation of f_0. The PFS maps and the statistical results are shown in Fig. S7 (SI). The *PR*-f_0 loops with various sampling points obtained from PVDF are shown in Fig. S8 (SI). The supplementary experiments and results also illustrate the stability of the ferroelectric-related f_0 variation during the PFS measurements.

Analysis of artifacts

In the PFS measurements, dual AC resonance tracking (DART) technique modulates the tip-sample contact at two frequencies (f_1 and f_2) where f_0 is located between the two. Each carrier frequency (f_1 or f_2) has the corresponding amplitude (A_1, A_2) and phase (ϕ_1, ϕ_2). Hence, f_0 can be calculated from the measurements of A_1, A_2, ϕ_1 and ϕ_2 [40]. According to the DHO model [41], the contact frequency f_0 can be expressed as:

$$f_0 = \sqrt{f_1 f_2 \frac{f_2 X_1 - f_1 X_2}{f_1 X_1 - f_2 X_2}}, \tag{1}$$

where

$$X_1 = -\frac{1-\mathrm{sgn}(\Phi)\sqrt{1+\Phi^2}/\Omega}{\Phi}, X_2 = \frac{1-\mathrm{sgn}(\Phi)\Omega\sqrt{1+\Phi^2}}{\Phi}, \tag{2}$$

and

$$\Omega \equiv \frac{f_1 A_1}{f_2 A_2}, \Phi \equiv \tan(\phi_1 - \phi_2). \tag{3}$$

In the DART-PFM measurements, it generally sets $A_1 = A_2$, hence, $\Omega = f_1/f_2$. Due to the fact that the width between f_1 and f_2 is a pre-set constant, X_1 and X_2 are related to the phase and frequency, except the amplitude. However, $A_1 = A_2$ is not the necessary condition in the DHO fitting [42]. In our experiments, the PFS measurements (performed by using MFP-3D, Oxford Instruments, CA, USA) actually use a constant ratio (A_1/A_2) instead of $A_1 = A_2$ as a feedback to adjust the values of f_1 and f_2. For a certain A_1/A_2 ratio, the calculation of f_0 can be described as $f_0(f_1, \Phi)$. Fig. 6(a) shows the calculated DHO fitting models at the fixed ratio of $A_1/A_2 = 0.36$; the calculations at other A_1/A_2 ratios are shown in Fig. S9 (SI). Note that the function, $f_0(f_1, \Phi)$, is not a continuous function, and f_0 goes to a peak point at $\Phi = 0$. When $\Phi \rightarrow +0$, f_0 is quickly rising to its peak value. When $\Phi \rightarrow -0$, f_0 is then dropping. For ideal model, f_0 can be accurately calculate at any Φ.

Compared with this simulated calculation, we also observe the relationship between f_1 and f_0 and the two signals of phase (ϕ_1 and ϕ_2) which are showed in Figs. 6 (b) and (c), and the table beside show the values of bias, f_0, Φ, ϕ_2-ϕ_1 of the four peaks, and the average value of all points from the measurements on BFO. The results obtained from other materials can be seen in Fig. S10 (SI). It is clear that, for ferroelectric materials, ϕ_2-ϕ_1 at all the peak positions are much lower than the average values. It illustrates that there is an obvious f_0 increase occurring in such a short time that the DART system cannot react in time to keep f_0 in the middle of dual frequencies. Therefore, ϕ_2-ϕ_1 becomes small but larger than zero (if it is less than zero, f_0 is missing after DHO calculation), which means f_0 goes to a larger value than the two tracking frequencies (f_1 and f_2) at the coercive bias. In spite of the slow tracking system, in some cases, the instantaneous increase of f_0 also can be captured by the feedback system. In Fig. S1(b) (SI), f_1 of PZN-PT shows two clear peaks at the coercive biases. After DHO fitting, f_0 always shows a clear peak at the position of coercive bias for ferroelectric materials. It can be interpreted as that f_1 and f_2 are at the same side of the resonance frequency. In other words, f_0 jumps to larger than f_2 when the domain is switched. For non-ferroelectric materials, ϕ_2-ϕ_1 values are far away from zero, and f_1-f_0 obeys the linear relationship. It means that, despite of the quick phase flipping [Fig. S2(c)], the DART system works stably, and f_0 do not show a large variation. To emphasize, all of the ferroelectric materials including Cu-doped ZnO, show significant reduction of ϕ_2-ϕ_1 during the polarization switching, and this should not be attributed by the machine noise or PFM artifacts.

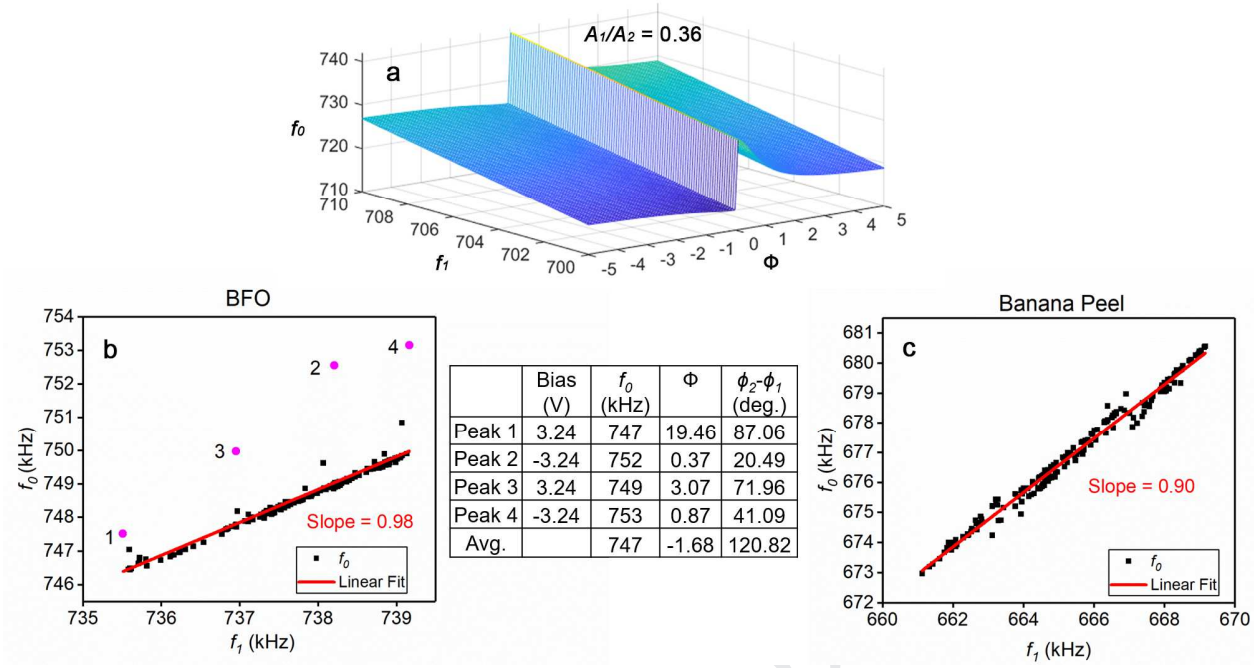

	Bias (V)	f_0 (kHz)	Φ	ϕ_2-ϕ_1 (deg.)
Peak 1	3.24	747	19.46	87.06
Peak 2	-3.24	752	0.37	20.49
Peak 3	3.24	749	3.07	71.96
Peak 4	-3.24	753	0.87	41.09
Avg.		747	-1.68	120.82

Fig. 6. (a) The f_0 values from simulated DHO model as functions of f_1 and Φ. The ratio of A_1/A_2 is 0.36. At Φ = 0, f_0 shows a significant peak value. f_1-f_0 relationship obtained from experiments for (b) BFO and (c) banana peel. Two cycles of the PFS measurements have been conducted on each sample; therefore, four peaks should appear in (a), which have been marked by pink dots and numbers indicating the order of the appearance. The bias, f_0, Φ, and ϕ_2-ϕ_1, of four peaks and the average value of all points can be seen in the right table of (b).

Another scanning mode SPM technique, contact resonance Atomic Force Microscopy (CR-AFM), tracks the contact resonance frequency as an indicator of the mechanical properties[43,44]. f_0 in the PFS measurements is also affected by the mechanical properties, though the contact mechanism is more complicated than that of the CR-AFM. It is anticipated that the difference of mechanical properties between the ferroelectric materials and non-ferroelectric materials can be reflected on the f_0 signals.

Furthermore, the effects of tracking errors (TEs) is analyzed at different DFWs using the analysis published by Bradler et al. TE and normalized TE is defined by Eqs.(S1) and (S2) (SI) [45].

Fig. S11 (SI) shows the time vs TE plots, which illustrates that the large DFW reduces TE. For both the ferroelectric and non-ferroelectric samples, the normalized TEs are usually around 0.4 if the DFW is larger than the FWHM. From the simulation results in the literature [45], it is known that the large TEs significantly affect the signals of A_0 and Q in the DART measurements; but for ϕ_d and f_0, the influence is small enough to be ignored. To confirm this, we plot the TE vs peak height as showed in Fig. S12 (SI). The results show that the f_0 peak height depends on the DFW but almost independent of the TE, which agrees with the literature report [45]. It is therefore believed that setting large DFW is more likely to accurately track the true f_0 values with a sudden jump when the local polarization is switching. This result also agrees with the study by Gannepalli et al. which reported the larger DFW increases the robustness of the contact resonance frequency tracking, especially when a sudden jump occurs [40]. Therefore, the obvious f_0 peaks occurring at large DFWs for ferroelectric materials prove that the observed pattern is not caused by artifacts in PFM during tracking or DHO fitting.

DISCUSSION

The contact resonance frequency in SPM is mainly related to the mechanical properties of the cantilever and the tip-sample contact stiffness [40,46,47]. During the PFM measurements, the oscillation of cantilever is indirectly driven by the AC bias-induced sample surface oscillation [43,48,49]. Hence, the instantaneous position of the tip in the vertical direction (z), obeys the driven damped harmonic oscillator equation as following [48]:

$$m_c \frac{d^2 z}{dt^2} = -k_c z - c_c \frac{dz}{dt} + F_{st} + F_d \cos \omega_d t \tag{4}$$

where F_d and ω_d are the amplitude and the angular frequency of the excitation force, respectively; m_c, k_c and c_c are the effective mass, the spring constant, and the viscous damping coefficient of the free

cantilever, respectively; F_{st} is the tip-sample interaction force, and it is mostly attributed by the Hertzian contact force. F_{st} can be expressed as [48]:

$$F_{st}(z) = \frac{4}{3} E^* \sqrt{R} (a_0 - z - z_c)^{\frac{3}{2}} \tag{5}$$

with

$$\frac{1}{E^*} = \frac{(1-\nu_t^2)}{E_t} + \frac{(1-\nu_s^2)}{E_s} \tag{6}$$

where R is the radius of the tip, E^* is the effective Young's modulus of the tip-sample contact system. E^* is related to the Young's modulus of the tip (E_t) and sample (E_s), and the Poisson's ratio of the tip (ν_t) and sample (ν_s). z_c is the equilibrium position of the cantilever. From Eqs. (2) and (3), it is obvious that F_{st} is related to the sample's mechanical properties. The system can be simplified by a damping harmonic oscillator (DHO) model [40,48] driven by the amplitude (A_d) and phase (ϕ_d) from the sample surface. In this case, the driving forces are transferred to a spring (k^*) and a dashpot (c) model in the system as showed in Fig. 7. The spring constant, k^*, is related to E^* by the following relation [50].

$$k^* = 2E^* r_c \tag{7}$$

where r_c is the radius of the contact area in the Hertz indentation model. f_0 is closely related to the ratio between the contact stiffness and the stiffness of the free cantilever (k^*/k_c). When k^*/k_c increases, $f_0/f_{0,c}$ (the ratio between the f_0 and the free cantilever frequency, $f_{0,c}$,) shifts from the free vibration to the clamped one; when the k^*/k_c value is over 100, $f_0/f_{0,c}$ arises significantly [48]. The relation between f_0 and k^* is:

$$\frac{f_0}{f_{0,c}} = \sqrt{\frac{k_c + k^*}{k_c}} \tag{8}$$

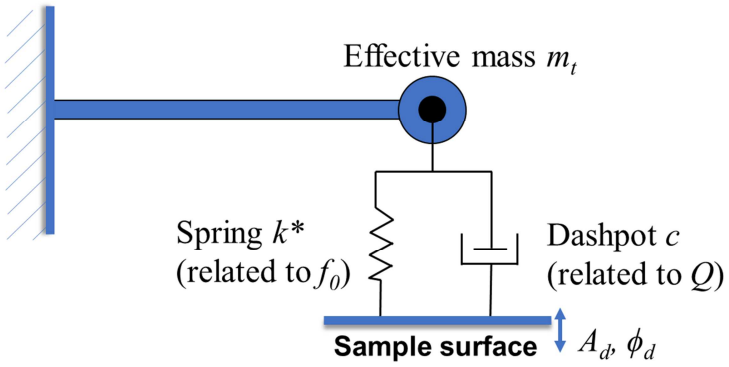

Fig. 7. A schematic diagram showing the tip-sample oscillating system: the forces between the tip and the sample surface can be represented by the spring k^*, and the damping can by represented by the dashpot c. m_t is the effective mass of the tip. k^* and c are related to the contact resonance frequency (f_0) and quality factor (Q), respectively. A_d and ϕ_d are the driving amplitude and phase from the sample surface, respectively.

In the earlier studies of the constitutive model for ferroelectric materials, it was found that the work-hardening effects should not be neglected [51]. A small hardening rate exists during the bias cycle processes. In this study, it is found that the contact resonance frequencies of ferroelectric materials increase constantly under the repetitive cyclic field (Fig. 5), this phenomenon may be related to the hardening effects in the ferroelectric materials. At macroscale, the ferroelectric fatigue behavior proves the hardening effect. The magnitude of the electrically-induced strain in the aged ferroelectric material is noticeably lower than that in the pristine one [52]. Combined with the analysis of the one-cycle results and ten-cycle results, it is believed that the hardening of ferroelectric materials is a non-linear process. On the other hand, for non-ferroelectric materials, the f_0 changes randomly with the poling voltage, which indicates no hardening processes, even though PFS measurements can get a similar hysteresis loop. The variations of f_0 in the ferroelectric materials and the non-ferroelectric materials were also observed by using CR-AFM [53], which are similar to that tracked by PFS.

From the experimental analysis and analysis based on Eqs.(3) to (5), it can be concluded that the increase of f_0 indicates the increase of the Young's modulus of the sample (E_s). Eventually, these variations affect the F_{st} as shown in the Eq.(1); hence, the oscillation of the cantilever is changed. The change of the sample's mechanical property may be caused by the small change of the materials structure during domain evolution. Highland et al. reported that the lattice parameter reaches a minimum when the polarization is switched in ferroelectric $PbTiO_3$ [54]. A smaller lattice may cause a higher stiffness, which may contribute to the instantaneous peak of f_0 in the PFS measurements for ferroelectric materials. Qin et al. also reported that the stress field may cause deviation of atoms from their ideal sites and change the lattice parameter for nanocrystalline materials [55]. It is therefore believed that this sharp increase is likely caused by an instantaneous increase of the Young's modulus of the sample at the moment when new domain is nucleated.

In this work, one of the materials, ZnO, should be further discussed in particular. ZnO is not a traditional ferroelectric material. However, domain switching and PFS hysteresis loop were observed in our previous work [56]. During the PFS measurements, not all of the points can obtain the hysteresis loop. However, at the locations where the hysteresis loop can be detected, f_0 changes similarly as that in the traditional ferroelectric materials. It is presumed that ZnO in thin film shape possess ferroelectricity, but the domain motion insider the thin film may not be as stable as that in the typical ferroelectric materials. By analyzing the variation of the contact resonance frequency in the PFS measurements, it is believed that the ferroelectric behavior in ZnO is clear but more complicated than that in the traditional ferroelectric materials.

SUMMARY AND CONCLUSION REMARKS

In summary, this study has investigated the variation of the contact resonance frequency during the polarization switching in the PFS measurements. Two groups of materials, including four

ferroelectric materials (PZN-PT, PVDF-Ag, BFO, doped ZnO), two non-ferroelectric materials (glass and banana peel) which have hysteresis loops, and an additional group of two non-ferroelectric materials (PMMA and Si) which have no hysteresis loops, were studied by PFS experiments. The PFS measurements have been conducted at (i) different DFWs; (ii) at off-field and on-field; and (iii) under multiple PFS cycles. In addition, the effect of the DHO fitting from the DART experiments has also been analyzed. The results have proved that the f_0-based method to differentiate ferroelectric materials and non-ferroelectric materials is very robust and effective. The variation of contact resonance frequency may be induced by the hardening effects during domain evolution in the ferroelectric materials. Therefore, an important feature of the ferroelectric behavior at nano- to micro-scales has been pointed out here, which can be considered as a new method to differentiate the real ferroelectric hysteresis loops from the ferroelectric-like loops of the non-ferroelectric materials during the PFS measurements. This study has also presented a new direction to characterize the ferroelectric responses and to decouple the contributing factors in the PFS measurements. In principle, the contact resonance frequency can be quantitatively interpreted into the stiffness or even Young's modulus if the value of the instantaneously high f_0 value is curate enough. It is believed that, with the advances of the technique of signal tracking and processing during the SPM measurements, the signal of the contact resonance frequency will reveal more characteristics and properties of ferroelectric materials in the future. We further speculate that it is possible to help to characterize the domain switching dynamics in the ferroelectric materials.

ASSOCIATED CONTENT

Supporting Information

A_1, f_1, DHO calculated ϕ_d, A_1/A_2 ratio and DFW of all the samples based on the data from the PFS measurements. Piezoresponse and amplitude of PZN-PT, BFO and glass at different DFWs. Tuned peaks of PZN-PT, BFO and glass. *PR*-f_0 curves at different locations. Definition of tracking errors. Normalized

tracking errors of PZN-PT, BFO, and glass. The relationship between TE and the peak height of f_0 on PZN-PT and BFO. PFS maps and statistical results on PZN-PT and BFO. *PR*-f_0 loops with various sampling points.

AUTHOR INFORMATION

Corresponding Authors

*Prof. Dr. Kaiyang Zeng, E-mail: mpezk@nus.edu.sg, Tel: (+65) 6516 6627, Fax (+65) 6779 1459.

Dr. Tao Li, E-mail: taoli66@xjtu.edu.cn, Tel: (+86) 29 82667957.

Author Contributions

The manuscript was written through contributions of all authors. YL performed all of the numerical analysis and wrote this manuscript. Other authors were contributed to the large amount of PFM and PFS experiments on various materials and discussions about the results and manuscript. All authors have given approval to the final version of the manuscript.

Funding Sources

This work is supported by Ministry of Education (Singapore) through National University of Singapore (NUS) under the Academic Research Fund (AcRF), R-265-000-596-112.

Notes

The authors declare no competing financial interest.

ACKNOWLEDGMENT

The authors would like to thank the financial support by Ministry of Education, Singapore, through National University of Singapore (NUS) under the Academic Research Fund (ARF) of grant number R-265-000-596-112. The authors (YL, YS, ZTW, BXY) also thanks the post-graduate scholarship provide by NUS; TL also thanks the support for post-doctoral research fellow from ARF of R-265-000-596-112 by Ministry of Education, Singapore.

ABBREVIATIONS

PFS, Piezoresponse Force Spectroscopy; PFM, Piezoresponse Force Microscopy; P-E, polarization-electric; SS-PFM, switching spectroscopy Piezoresponse Force Microscopy; CR-AFM, contact resonance Atomic Force Microscopy; SHG, second harmonic generation; cKPFM, contact Kelvin Probe Force Microscopy; DHO, damping harmonic oscillator; SPM, Scanning Probe Microscopy; DART, dual AC resonance tracking; DFW, DART frequency width; BE, band exciation; SNR, signal to noise ratio; AFAM, Atomic Force Acoustic Microscopy; AFM, Atomic Force Microscopy; PR, piezoresponse; FWHM, full width at half maximum; TE, tracking error; PZN-PT, $Pb(Zn_{1/3}Nb_{2/3})O_3$–9%$PbTiO_3$; CR-FM, contact resonance frequency Atomic Force Microscopy; PVDF-Ag, hybrid polymeric-metallic; BFO, $BiFeO_3$; PMMA, Poly(methyl methacrylate).

REFERENCES

[1] Lines ME, Glass AM. Principles and Applications of Ferroelectrics and Related Materials. OUP Oxford; 1977.

[2] Whatmore R. Ferroelectric Materials. In: Kasap S, Capper P, editors. Springer Handb. Electron. Photonic Mater., Cham: Springer International Publishing; 2017, p. 1–1. https://doi.org/10.1007/978-3-319-48933-9_26.

[3] Xu K, Lu X-Z, Xiang H. Designing new ferroelectrics with a general strategy. Npj Quantum Mater 2017;2:1–6. https://doi.org/10.1038/s41535-016-0001-8.

[4] Garrity KF. High-throughput first principles search for new ferroelectrics. Phys Rev B 2018;97. https://doi.org/10.1103/PhysRevB.97.024115.

[5] Kalinin SV, Morozovska AN, Chen LQ, Rodriguez BJ. Local polarization dynamics in ferroelectric materials. Rep Prog Phys 2010;73:056502. https://doi.org/10.1088/0034-4885/73/5/056502.

[6] Jesse S, Lee HN, Kalinin SV. Quantitative mapping of switching behavior in piezoresponse force microscopy. Rev Sci Instrum 2006;77:073702. https://doi.org/10.1063/1.2214699.

[7] Strelcov E, Kim Y, Yang JC, Chu YH, Yu P, Lu X, et al. Role of measurement voltage on hysteresis loop shape in Piezoresponse Force Microscopy. Appl Phys Lett 2012;101:192902. https://doi.org/10.1063/1.4764939.

[8] Roelofs A, Böttger U, Waser R, Schlaphof F, Trogisch S, Eng LM. Differentiating 180° and 90° switching of ferroelectric domains with three-dimensional piezoresponse force microscopy. Appl Phys Lett 2000;77:3444–6. https://doi.org/10.1063/1.1328049.

[9] Miao H, Tan C, Zhou X, Wei X, Li F. More ferroelectrics discovered by switching spectroscopy piezoresponse force microscopy? EPL Europhys Lett 2014;108:27010. https://doi.org/10.1209/0295-5075/108/27010.

[10] Alexe M, Gruverman A. Nanoscale Characterisation of Ferroelectric Materials: Scanning Probe Microscopy Approach. Springer Science & Business Media; 2013.

[11] Kalinin SV, Gruverman A, Rodriguez BJ, Shin J, Baddorf AP, Karapetian E, et al. Nanoelectromechanics of polarization switching in piezoresponse force microscopy. J Appl Phys 2005;97:074305. https://doi.org/10.1063/1.1866483.

[12] Polomoff NA, Nath R, Bosse JL, Huey BD. Single ferroelectric domain nucleation and growth monitored by high speed piezoforce microscopy. J Vac Sci Technol B Microelectron Nanometer Struct 2009;27:1011. https://doi.org/10.1116/1.3077485.

[13] Jesse S, Baddorf AP, Kalinin SV. Switching spectroscopy piezoresponse force microscopy of ferroelectric materials. Appl Phys Lett 2006;88:062908. https://doi.org/10.1063/1.2172216.

[14] Shvartsman VV, Pertsev NA, Herrero JM, Zaldo C, Kholkin AL. Nonlinear local piezoelectric deformation in ferroelectric thin films studied by scanning force microscopy. J Appl Phys 2005;97:104105. https://doi.org/10.1063/1.1891273.

[15] Sanwlani S, Balal M, Jyotsna S, Sheet G. The role of substrates and environment in piezoresponse force microscopy: A case study with regular glass slides. Solid State Commun 2016;246:17–22. https://doi.org/10.1016/j.ssc.2016.07.023.

[16] Kalinin SV, Bonnell DA. Contrast Mechanism Maps for Piezoresponse Force Microscopy. J Mater Res 2002;17:936–9. https://doi.org/10.1557/JMR.2002.0138.

[17] Balke N, Maksymovych P, Jesse S, Kravchenko II, Li Q, Kalinin SV. Exploring Local Electrostatic Effects with Scanning Probe Microscopy: Implications for Piezoresponse Force Microscopy and Triboelectricity. ACS Nano 2014;8:10229–36. https://doi.org/10.1021/nn505176a.

[18] Li Q, Liu Y, Wang D, Withers RL, Li Z, Luo H, et al. Switching spectroscopic measurement of surface potentials on ferroelectric surfaces via an open-loop Kelvin probe force microscopy method. Appl Phys Lett 2012;101:242906. https://doi.org/10.1063/1.4772511.

[19] Chen QN, Ou Y, Ma F, Li J. Mechanisms of electromechanical coupling in strain based scanning probe microscopy. Appl Phys Lett 2014;104:242907. https://doi.org/10.1063/1.4884422.

[20] Balke N, Jesse S, Morozovska AN, Eliseev E, Chung DW, Kim Y, et al. Nanoscale mapping of ion diffusion in a lithium-ion battery cathode. Nat Nanotechnol 2010;5:749–54. https://doi.org/10.1038/nnano.2010.174.

[21] Balke N, Jesse S, Kim Y, Adamczyk L, Tselev A, Ivanov IN, et al. Real Space Mapping of Li-Ion Transport in Amorphous Si Anodes with Nanometer Resolution. Nano Lett 2010;10:3420–5. https://doi.org/10.1021/nl101439x.

[22] Balke N, Kalnaus S, Dudney NJ, Daniel C, Jesse S, Kalinin SV. Local Detection of Activation Energy for Ionic Transport in Lithium Cobalt Oxide. Nano Lett 2012;12:3399–403. https://doi.org/10.1021/nl300219g.

[23] Proksch R. Electrochemical strain microscopy of silica glasses. J Appl Phys 2014;116:066804. https://doi.org/10.1063/1.4891349.

[24] Kim Y, Jang JH, Park S-J, Jesse S, Donovan L, Borisevich AY, et al. Local probing of electrochemically induced negative differential resistance in TiO_2 memristive materials. Nanotechnology 2013;24:085702. https://doi.org/10.1088/0957-4484/24/8/085702.

[25] Scott JF. Ferroelectrics go bananas. J Phys Condens Matter 2008;20:021001. https://doi.org/10.1088/0953-8984/20/02/021001.

[26] Vasudevan RK, Balke N, Maksymovych P, Jesse S, Kalinin SV. Ferroelectric or non-ferroelectric: Why so many materials exhibit "ferroelectricity" on the nanoscale. Appl Phys Rev 2017;4:021302. https://doi.org/10.1063/1.4979015.

[27] Denev SA, Lummen TTA, Barnes E, Kumar A, Gopalan V. Probing Ferroelectrics Using Optical Second Harmonic Generation. J Am Ceram Soc 2011;94:2699–727. https://doi.org/10.1111/j.1551-2916.2011.04740.x.

[28] Neacsu CC, van Aken BB, Fiebig M, Raschke MB. Second-harmonic near-field imaging of ferroelectric domain structure of $YMnO_3$. Phys Rev B 2009;79:100107. https://doi.org/10.1103/PhysRevB.79.100107.

[29] Tenne DA, Bruchhausen A, Lanzillotti-Kimura ND, Fainstein A, Katiyar RS, Cantarero A, et al. Probing Nanoscale Ferroelectricity by Ultraviolet Raman Spectroscopy. Science 2006;313:1614–6. https://doi.org/10.1126/science.1130306.

[30] Jia C-L, Nagarajan V, He J-Q, Houben L, Zhao T, Ramesh R, et al. Unit-cell scale mapping of ferroelectricity and tetragonality in epitaxial ultrathin ferroelectric films. Nat Mater 2007;6:64–9. https://doi.org/10.1038/nmat1808.

[31] Balke N, Maksymovych P, Jesse S, Herklotz A, Tselev A, Eom C-B, et al. Differentiating Ferroelectric and Nonferroelectric Electromechanical Effects with Scanning Probe Microscopy. ACS Nano 2015;9:6484–92. https://doi.org/10.1021/acsnano.5b02227.

[32] Seol D, Park S, Varenyk OV, Lee S, Lee HN, Morozovska AN, et al. Determination of ferroelectric contributions to electromechanical response by frequency dependent piezoresponse force microscopy. Sci Rep 2016;6:30579. https://doi.org/10.1038/srep30579.

[33] Wang H, Zeng K. Domain structure, local surface potential distribution and relaxation of $Pb(Zn_{1/3}Nb_{2/3})O_3$–9%$PbTiO_3$ (PZN–9%PT) single crystals. J Materiomics 2016;2:309–15. https://doi.org/10.1016/j.jmat.2016.08.001.

[34] Liow CH, Lu X, Tan CF, Chan KH, Zeng K, Li S, et al. Spatially Probed Plasmonic Photothermic Nanoheater Enhanced Hybrid Polymeric-Metallic PVDF-Ag Nanogenerator. Small 2017:1702268. https://doi.org/10.1002/smll.201702268.

[35] Xiao J, Herng TS, Ding J, Zeng K. Resistive switching behavior in copper doped zinc oxide (ZnO:Cu) thin films studied by using scanning probe microscopy techniques. J Alloys Compd 2017;709:535–41. https://doi.org/10.1016/j.jallcom.2017.03.169.

[36] Cheng J-R, Eitel R, Cross LE. Lanthanum-Modified (1- x)$(Bi_{0.8}La_{0.2})(Ga_{0.05}Fe_{0.95})O_3 \cdot xPbTiO_3$ Crystalline Solutions: Novel Morphotropic Phase-Boundary Lead-Reduced Piezoelectrics. J Am Ceram Soc 2003;86:2111–5. https://doi.org/10.1111/j.1151-2916.2003.tb03617.x.

[37] Hong S, Woo J, Shin H, Jeon JU, Pak YE, Colla EL, et al. Principle of ferroelectric domain imaging using atomic force microscope. J Appl Phys 2000;89:1377–86. https://doi.org/10.1063/1.1331654.

[38] Soergel E. Piezoresponse force microscopy (PFM). J Phys Appl Phys 2011;44:464003. https://doi.org/10.1088/0022-3727/44/46/464003.

[39] Mallat SG. A wavelet tour of signal processing: the sparse way. 3rd ed. Amsterdam ; Boston: Elsevier/Academic Press; 2009.

[40] Gannepalli A, Yablon DG, Tsou AH, Proksch R. Mapping nanoscale elasticity and dissipation using dual frequency contact resonance AFM. Nanotechnology 2011;22:355705.

[41] French AP. Vibrations and Waves. CRC Press; 2017. https://doi.org/10.1201/9781315273372.

[42] Rodriguez BJ, Callahan C, Kalinin SV, Proksch R. Dual-frequency resonance-tracking atomic force microscopy. Nanotechnology 2007;18:475504. https://doi.org/10.1088/0957-4484/18/47/475504.

[43] Stan G, Solares SD. Frequency, amplitude, and phase measurements in contact resonance atomic force microscopies. Beilstein J Nanotechnol 2014;5:278–88. https://doi.org/10.3762/bjnano.5.30.

[44] Stan G, Krylyuk S, Davydov AV, Vaudin MD, Bendersky LA, Cook RF. Contact-resonance atomic force microscopy for nanoscale elastic property measurements Spectroscopy and imaging 2009:8.

[45] Bradler S, Schirmeisen A, Roling B. Piezoresponse force and electrochemical strain microscopy in dual AC resonance tracking mode: Analysis of tracking errors. J Appl Phys 2018;123:035106. https://doi.org/10.1063/1.5004472.

[46] Yamanaka K, Nakano S. Quantitative elasticity evaluation by contact resonance in an atomic force microscope. Appl Phys A 1998;66:S313–7. https://doi.org/10.1007/s003390051153.

[47] Harnagea C, Alexe M, Hesse D, Pignolet A. Contact resonances in voltage-modulated force microscopy. Appl Phys Lett 2003;83:338–40. https://doi.org/10.1063/1.1592307.

[48] Rabe U, Janser K, Arnold W. Vibrations of free and surface□coupled atomic force microscope cantilevers: Theory and experiment. Rev Sci Instrum 1996;67:3281–93. https://doi.org/10.1063/1.1147409.

[49] Rabe U, Kester E, Arnold W. Probing linear and non-linear tip–sample interaction forces by atomic force acoustic microscopy. Surf Interface Anal 1999;27:386–91. https://doi.org/10.1002/(SICI)1096-9918(199905/06)27:5/6<386::AID-SIA526>3.0.CO;2-J.

[50] Garcia R, Proksch R. Nanomechanical mapping of soft matter by bimodal force microscopy. Eur Polym J 2013;49:1897–906. https://doi.org/10.1016/j.eurpolymj.2013.03.037.

[51] Huber J e., Fleck N a., Landis CM, McMeeking RM. A constitutive model for ferroelectric polycrystals. J Mech Phys Solids 1999;47:1663–97. https://doi.org/10.1016/S0022-5096(98)00122-7.

[52] Priya S, Kim HW, Ryu J, Zhang S, Shrout TR, Uchino K. Modeling of fatigue behavior in relaxor piezocrystals: Improved characteristics by Mn substitution. J Appl Phys 2002;92:3923–7. https://doi.org/10.1063/1.1503411.

[53] Li Q, Jesse S, Tselev A, Collins L, Yu P, Kravchenko I, et al. Probing Local Bias-Induced Transitions Using Photothermal Excitation Contact Resonance Atomic Force Microscopy and Voltage Spectroscopy. ACS Nano 2015;9:1848–57. https://doi.org/10.1021/nn506753u.

[54] Highland MJ, Fister TT, Richard M-I, Fong DD, Fuoss PH, Thompson C, et al. Polarization Switching without Domain Formation at the Intrinsic Coercive Field in Ultrathin Ferroelectric PbTiO 3. Phys Rev Lett 2010;105:167601. https://doi.org/10.1103/PhysRevLett.105.167601.

[55] Qin W, Nagase T, Umakoshi Y, Szpunar JA. Relationship between microstrain and lattice parameter change in nanocrystalline materials. Philos Mag Lett 2008;88:169–79. https://doi.org/10.1080/09500830701840155.

[56] Herng TS, Wong MF, Qi D, Yi J, Kumar A, Huang A, et al. Mutual Ferromagnetic–Ferroelectric Coupling in Multiferroic Copper-Doped ZnO. Adv Mater 2011;23:1635–40. https://doi.org/10.1002/adma.201004519.

Highlight

- Significant differences in contact resonances during DART-PFS measurements in ferro- and non-ferroelectric materials.
- A new unique feature for the ferroelectric materials during the DART-PFS measurement.
- An analysis to differentiate the responses from the ferroelectric and non-ferroelectric materials

Variation of Contact Resonance Frequency during Domain Switching in DART-PFM Measurements for Ferroelectric Materials

Yue Liu, Yao Sun, Wanheng Lu, Hongli Wang, Zhongting Wang, Bingxue Yu, Tao Li,[*,#]

Kaiyang Zeng[*]

About authors:

Ms. Yue Liu is currently the Ph.D student at Department of Mechanical Engineering, National University of Singapore (NUS). She received her B. S. degree in Engineering Mechanics in 2014 from Wuhan University and M. S. degree in 2017 from Dalian University of Technology, China. Her research focuses on the data analysis and artificial intelligence applications to Scanning Probe Microscopy image analysis.

Dr. Yao Sun is a Research Fellow at Department of Mechanical Engineering, NUS. She obtained her Ph.D degree from Department of Mechanical Engineering, NUS in May 2019. Her current research is mainly focused on study the functionality of biomaterials and hybrid materials by using Scanning Probe Microscopy Techniques and molecular simulations.

Dr. Wanheng Lu is a Research Fellow at Department of Electrical and Computer Engineering, and Department of Mechanical Engineering, NUS. She obtained her Ph.D. degree from Department of Mechanical Engineering, NUS in 2017. Her current research interests include synthesis and characterization of functional nanomaterials in the field of clean and renewable energy, and applications of Scanning Probe Microscopy (SPM) techniques.

Dr. Hongli Wang is a research scientist at Guangdong Institute of New Materials, China. She obtained her Ph.D degree from Department of Mechanical Engineering, NUS in December 2017. Her current research is mainly focused on the piezoelectric and ferroelectric materials by using Scanning Probe Microscopy Techniques.

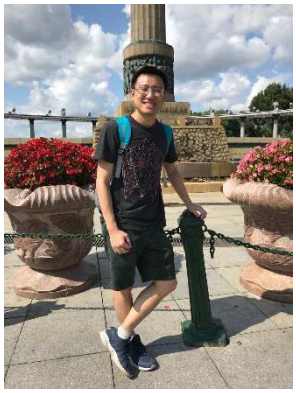

Mr. Zhongting Wang is current a Ph.D student at Department of Mechanical Engineering, NUS. He obtained his bachelor's degree and master's degree from Department of

Astronautics, Harbin Institute of Technology. His current research is mainly focused on the study of the functional materials of lithium ion battery by using Scanning Probe Microscopy Techniques and Molecular Dynamics.

Ms. Bingxue Yu is currently the Ph.D student at Department of Mechanical Engineering, NUS. She obtained her B. S. degree in Engineering Mechanics in 2016 from Huazhong University of Science and Technology. Her research mainly focuses on characterizing the memory behaviours of transition metal oxides and revealing the mechanisms by Scanning Probe Microscopy techniques.

Dr. Tao Li is an Associate Professor at the School of Materials Science and Engineering, Xi'an Jiaotong University. She obtained her Ph. D in Mechanical Engineering from NUS in 2013, and had spent 3 years for postdoctoral research at the Department of Physics and Astronomy, University of Nebraska-Lincoln, USA. Her current research interest is the interfacial multi-field coupling effects for non-volatile digital memory applications.

Dr. Kaiyang Zeng is Associate Professor at Department of Mechanical Engineering, NUS. He got his Ph.D in materials science from Royal Institute Technology (KTH), Sweden. His main

research areas include using Scanning Probe Microscopy based techniques to study the multifield coupling phenomena in advanced materials, such as high performance piezo/ferroelectric materials, biomaterials, supramolecular materials, oxide materials, and energy storage materials. Dr. Zeng has published more than 200 journal papers and with H-index of 37.

The authors declare no competing financial interest.